

Multiscale approach to radiation damage induced by ion beams: complex DNA damage and effects of thermal spikes

E. Surdutovich^{1, 2a}, A. V. Yakubovich^{1,3}, and A. V. Solov'yov^{1, 3b}

¹ Frankfurt Institute for Advanced Studies, Ruth-Moufang-Str. 1, 60438 Frankfurt am Main, Germany

² Department of Physics, Oakland University, Rochester, Michigan 48309, USA

³ On leave from A.F. Ioffe Physical-Technical Institute, 194021 St. Petersburg, Russia

October 17, 2018

Abstract. We present the latest advances of the multiscale approach to radiation damage caused by irradiation of a tissue with energetic ions and report the most recent advances in the calculations of complex DNA damage and the effects of thermal spikes on biomolecules. The multiscale approach aims to quantify the most important physical, chemical, and biological phenomena taking place during and following irradiation with ions and provide a better means for clinically-necessary calculations with adequate accuracy. We suggest a way of quantifying the complex clustered damage, one of the most important features of the radiation damage caused by ions. This method can be used for the calculation of irreparable DNA damage. We include thermal spikes, predicted to occur in tissue for a short time after ion's passage in the vicinity of the ions' tracks in our previous work, into modeling of the thermal environment for molecular dynamics analysis of ubiquitin and discuss the first results of these simulations.

PACS. 61.80.-x Physical radiation effects, radiation damage – 87.53.-j Effects of ionizing radiation on biological systems – 41.75.Ak Positive-ion beams – 87.15.ap Molecular dynamics simulation

1 Introduction

The success of heavy-ion-beam therapies, employed in Germany and Japan, stems from several advantages of these

therapies over the common photon therapies [1, 2, 3]. These advantages can be described in the following way. First, the Bragg peak in the linear energy transfer (LET) dependence on the penetration depth gives an opportunity to better localize the dose distribution on the targeted area.

^a E-mail: surdutov@oakland.edu; Tel: +1-248-370-3409

^b E-mail: solovyov@fias.uni-frankfurt.de

Provided that the targeted radiation damage requires this dose, the overall delivered dose in ion-beam therapy is smaller. This makes the ratio of the the doses delivered by photons to that of ions (the (overall) relative biological effectiveness (RBE)) larger than one (if there is no significant overkill effect in the Bragg peak region). This advantage is substantiated by the possibility of achieving relatively sharp edges in the dose distribution, which spares vital organs, not touched by the tumor, from irradiation, thus reducing side effects. Second, the concentration of radiation damage caused by high-LET ion irradiation is significantly larger than that of photon irradiation. This changes the radiation damage not only quantitatively (by increasing the dose localization) but qualitatively as well, i.e., the pathways of radiation damage change so that the direct effects dominate the indirect ones. This solves the problem of cell resistivity to irradiation and increases the local RBE, even for hypoxic tumors.

Despite the successes of ion therapies there are many unanswered questions. The scenario of events from the incidence of an ion onto tissue to the cell death is vague. Some important processes are not understood even on a qualitative level. Given that the radiation damage to DNA is mostly responsible for cell death [4,5,6,7], the pathways of this damage are not sufficiently quantified. The roles of different factors are still being evaluated. The approaches to calculating the local RBE, like the Local Effect Model [8,9,10], which is based on local dose with an ad-hoc accounting for complex damage, may be sufficient for now; but, the future of ion-beam therapies requires a

more sound phenomenological (if not an *ab initio*) calculation of the RBE. The main obstacle to understanding radiation damage to DNA on the microscopic level is that the scenario includes events on many spatial, temporal, and energetic scales; e.g., time scales for relevant processes vary from 10^{-22} s to minutes, hours, or even longer times. Indeed, 10^{-22} s is the characteristic time of nuclear reactions, which take place when an incident ion collides with nuclei of the medium; 10^{-17} s is that of ionization and excitation of molecules of the medium, which are the leading processes of energy loss by the projectile, 10^{-12} s is that of the transport of secondary electrons formed as a result of the above ionization, 10^{-5} s is that of DNA damage, and longer times correspond to DNA repair by different mechanisms. These scales are presented in Table 1.

The claim of our multiscale approach to the physics of ion-beam cancer therapy is that the phenomenon-based calculation of the RBE is possible if we evaluate the most important physical, chemical, and biological effects that happen in the process of irradiation and (mainly biological) processes following irradiation on longer time scales. Instead of reconstructing the sequence of events using scale-dependent Monte Carlo (MC) simulations, we consider phenomena on all scales and combine them in a complete picture [11,12,13,14,15,16,17].

The understanding of the scenario of DNA damage and repair is an interdisciplinary science problem, and its whole scope is shown in Table 1. From this table, one can see that this problem joins different areas of physics, chemistry, and biology. This scope is too vast for taking on

Table 1. Disciplines and scales of ion-beam cancer therapy

Phenomenon	Discipline	Space scale	Time scale
Beam generation	High energy physics	m–km	
Beam transport	Radiation physics	1–100 cm	10^{-7} s
Nuclear collisions and fragmentation	Nuclear physics	fm	10^{-22} s
Primary ionization, transport of secondaries	Atomic/molecular physics	0.1–10 nm	$10^{-17} - 10^{-12}$ s
Branching of secondaries, radicals, excited species, chemical equilibrium	Chemistry	1–10 nm	$10^{-12} - 10^{-5}$ s
Local heating, heat transfer, stress	Thermo/hydro-dynamics	1–10 nm	$10^{-14} - 10^{-9}$ s
Dissociative electron attachment to molecules and other reactions	Quantum chemistry	Å	10^{-15} s
Initial damage effects	Biochemistry	0.1–10 nm	10^{-5} s
Repairing mechanisms	Molecular biology	1–100 nm	s–min
Cellular network and interaction	Cell biology	μ m	min
(Tumor) Cell death	Medicine	mm	min–years

all scales simultaneously, and in the beginning we limited our considerations to physical and some chemical phenomena. At this moment, our multiscale approach consists of analyses of ion propagation in a medium, production and transport of secondary electrons, and different pathways of DNA damage and their quantification.

We continue this paper with a quick overview of ion transport and production of secondary electrons in Section 2. Then we address several issues of DNA damage in Section 3. Two subsections in that section, on cluster damage and on the effect of thermal spikes on ubiquitin, are new steps in our development of the multiscale approach.

2 Ion stopping and production of secondary electrons

Energetic ions incident on tissue lose energy primarily through ionization of molecules of the medium. The main characteristic, which describes the phenomena on this scale (by far the longest spatial) is the singly differential (in the energy of released electrons) cross section of ionization (SDCS) [12]. This cross section is proportional to the energy distribution of secondary electrons, which is, in its turn, important for the calculation of DNA damage. For the ion's transport, the first moment of the SDCS along with the excitation cross section contributes to the total energy loss or stopping cross section. For many purposes, the LET, inversely proportional to the stopping cross sec-

tion, is a more convenient characteristic. Most important, the LET dependence on the depth in tissue gives the longitudinal dose distribution, which is directly related to the radiation damage. The Bragg peak in the LET dependence on depth, a sharp maximum close to the end of the ion's track, is a major contribution to the advantages of ion-beam therapies.

The subsequent DNA damage is done either by the secondary electrons, produced at this stage [18,19,20,21], or by the holes (also produced as a result of the ionization of the medium); these comprise the direct and quasi-direct effects [18,22,19,20]. The indirect effect is caused by hydroxyl radicals resulted from ionization and excitation of the medium. The direct effects are more important when tissue is irradiated with heavy ions; their relative independence from the chemical properties of the medium (such as the presence of oxygen) is particularly attractive for treatment of hypoxic tumors. The interaction of secondary electrons with DNA is defined by their energy and number density at the location of the DNA molecule. The transport properties, such as the mean free path of electrons, are also energy-dependent. Therefore, the energy spectrum of the secondary electrons is very much desired. It turns out, however, that at low energies, this distribution, in a medium such as liquid water, is neither easy to calculate, nor measure experimentally. We have gradually improved our approach to calculating these spectra in Refs. [11,12,17]. In Ref. [17] we have improved the parametric approach at low energies of projectiles and analyzed different options at high energies.

Note, that the dose concentration does not yet mean the reduction of the dose. Thus far, it is assumed that the damage is proportional to the dose, i.e., in order to eradicate a desired percentage of cells in a given region the same dose is required there, whatever the projectile is. However, due to dose localization in ion therapies, the dose in the surrounding regions is smaller than that in photon therapy; therefore the overall RBE increases.

3 Pathways of DNA damage

The localization of dose associated with the Bragg peak results in a high number density of secondary electrons. This results in complex DNA damage [23,24]. The complex damage reduces the capabilities of proteins to repair the damage. Thus, the damage induced in high-LET irradiation is more lethal to the cells. This adds a new quality to the dose and poses a question of what is more important, the energy or complexity of damage. This quality enhances the RBE locally and makes up still another advantage of ion-beam therapies. This advantage is more related to chemistry and biology even though it is a consequence of physical effects.

3.1 Estimation of DNA damage done by secondary electrons

In order to quantify the second feature of high-LET irradiation, one needs to investigate the pathways and mechanisms of DNA damage and repair. It is widely accepted that double-strand breaking (DSB) is the most pernicious

type of DNA damage. This damage is defined as the breaking of both strands of DNA on the length of a single DNA convolution. It is also known that an isolated DSB can be repaired; however if additional lesions occur nearby, i.e., if damage is clustered sufficiently, it may be lethal for the cell. A single-strand break (SSB) can easily be repaired; but, if several of them happen close enough together (not causing a DSB) then the so-called multiple strand break may also result in irreparable damage.

Using the results of Refs. [25,26,27,21], we considered the diffusion of low-energy secondary electrons from the place of their origin to the DNA [14]. This work showed that the probability of a particular DNA convolution to encounter a secondary electron, is strongly dependent on the distance from the convolution to the ion's path, and only slightly depends on the orientation of the convolution with respect to the ion's path. This result has let us make an estimate of a number of DSBs caused by an ion's passage through a cell nucleus. An estimate was made for carbon ions passing through glial cells, which comprise 90% of the human brain. It predicted 3.5 DSBs per μm of the ion's track in the vicinity of the Bragg peak [14]. This number can be very reasonably compared with the number, 2.6 DSBs per μm , reported by experimental studies of Taucher-Scholz et al. at GSI [28]. However, these are only the first crude estimates. They only consider one pathway of DNA damage. For the probability of the DSB yield in an electron-DNA collision, we relied on the experimental data of Sanche [21]. These famous experiments, however, may not represent the whole picture, because the DNA

used in these experiments had not been hydrated as it is *in vivo* and its properties, such as the probability of a DSB after being hit by an electron, may be different. More research is required in order to better quantify this pathway. Other pathways include damage done by holes formed in the process of ionization, possible damage due to the temperature increase in the vicinity of the beam, the damage done by radicals, and all possible combinations of the above.

3.2 Calculation of clustered damage

As we have already pointed out, the damage complexity is one of the consequences of the so-called high-LET irradiation because in regions where the LET is high, many agents of damage are produced. This increases the probability of several agents, such as secondary electrons, holes, and hydroxyl radicals, to make lesions in the adjacent regions of DNA. Such lesions, SSBs, DSBs, and base damage, combined together on a distance of less than 100 bp make up the complex damage sites. While biologists study the pathways of repair of such sites [29,30], biological physicists investigate the cause of such damage [31, 32]. In this work, we want to quantify the complex damage without MC simulations. Such a quantification is an important part of our multiscale approach to radiation damage.

Imagine an ion, near its Bragg peak, passing through a cell nucleus. It ionizes the tissue, and secondary electrons, holes, and formed radicals cause DNA damage in the vicinity of the track. The damage may be clustered;

i.e., along the track there are some SSBs, DSBs, oxidative base damages, abasic sites, and combinations thereof. Then, within minutes, the repair mechanisms become active: H2AX histone becomes phosphorylated (γ -H2AX) and e.g., attracts such repair agents as proteins 53BP1, NBS1 and MDC1. These γ -H2AX-centered aggregations, called “foci”, are observed and remain until the DNA is repaired [28].

In general, it may not be easy to classify different cluster damage, because there are too many different possibilities [31,32]. We suggest classifying clusters by the number of independent agents, which cause the damage. For simplicity we will assume, for now, that only secondary electrons cause damage to DNA. For example, if a single secondary electron brings about a DSB and nothing else is damaged within certain region, we will refer to such a site as a singly-damaged site (DS1). If two electrons damage a DNA molecule within a certain distance, we will refer to this as a doubly-damaged site (DS2). In this case, the condition, which defines the maximum distance between the lesions is that only one repair focus is formed to repair the site. Then we can similarly introduce DS3, DS4, etc.

Thus, in order to approach the clustered damage, we should only consider the lesions due to a single electron, such as SSBs, DSBs, base damage, etc., with certain energy-dependent probabilities. Then, since secondary electrons are mutually independent, we can calculate the probability of clustered damage, such as DS1, DS2, etc., using Poisson statistics.

Let us consider one example of such a calculation for a superficial case where each electron causes a DSB with a certain probability and these DSBs may be clustered. This example is based on the probability of DSBs caused by secondary electrons [14]. Let us suppose that each DSB can be surrounded by some volume, such that, if any other DSB occurs within this volume, it will be counted as a member of the same cluster (e.g., if there are no other DSBs within this volume then this will be a cluster containing just one DSB, i.e., DS1). Let us denote this volume as V_C . Let the probability of a single DSB occurring inside this volume be $p(1)$. The probability of two DSBs occurring within this volume is $p(2)$, that of three DSBs is $p(3)$, etc. Let us now calculate these probabilities, taking the volume of the cluster V_C to be the volume of one nucleosome bead consisting of eight histones wrapped by a stretch of DNA consisting of 146 bp. This seems to be a reasonable unit related to DNA geometry, and the number of bp involved is of the order of the upper limit of the modeled cluster damage [31,32].

According to the method of calculating the number of DSBs per convolution volume [14], overviewed above, this number (for glial cells with a convolution right next to the ion’s track) is $N_{conv} \approx 3 \times 10^{-3}$). As in that work, we assume that the DNA is uniformly distributed inside cell nuclei. This assumption is reasonable for cells in their interphase, where they spend most of their life. We can translate this number into an average number of DSBs per cluster volume $N_C = N_{conv} n_{conv} V_C$, where $n_{conv} = 4 \times 10^6 \mu\text{m}^{-3}$ is the number density of convolutions inside

the cell nucleus (for glial cells). Then $N_C = 1.2 \times 10^{-2}$ (for $V_C=10^{-6} \mu\text{m}^3$) and the probability of exactly k DSBs to occur in this volume, $p(k)$, is given by the Poisson distribution:

$$p(k) = \exp(-N_C) \frac{N_C^k}{k!}. \quad (1)$$

With the above N_C , $p(1) = 1.2 \times 10^{-2}$, $p(2) = 7.1 \times 10^{-4}$, and so on. Neither $p(1)$ nor $p(2)$ depends on time. If this comparison works, it proves that the above picture of damage is correct and the average number of DSBs per cluster can be inferred (in this idealized case) from the ratio of these probabilities:

$$N_C = 2 \frac{p(2)}{p(1)}. \quad (2)$$

Notice that the volume of the cluster V_C is many times smaller than the volume of a focus, $\approx 1 \mu\text{m}^3$ [28]. The latter corresponds to the volume occupied by all proteins engaged in the repair process. Our assumption that the cluster volume is that of a nucleosome bead is not important for the suggested analysis and the size of a cluster can be changed if necessary. For example, let us take the cluster volume to be 100 times larger than the volume of a nucleosome, then $N_C = 1.2$, and corresponding $p(1)$ and $p(2)$ are 7.8×10^{-2} and 9.1×10^{-2} , respectively. The ratio given by eq. (2) still holds and does not alter the logic of the suggested method. However, if V_C turns out to be too large ($1 \mu\text{m}^3$) then the probability of having just one or two lesions will be unreasonably small. In this case, the whole concept of the clustered damage will have to be reconsidered, since the number of DSBs per cluster will be in triple digits. In general, it is the repair mechanism

that defines the V_C , and thus, it may be smaller than the volume of the nucleosome as well.

The reality is less straightforward than the considered example for at least two reasons: each electron may cause different types of lesions with different probabilities, and there is more than one pathway of DNA damage. Both of these complications can be overcome in the following way. In order to describe different types of lesions due to different agents, we can introduce the probabilities $p_{11}, p_{12}, p_{13}, \dots, p_{21}, p_{22}, p_{23}, \dots, p_{31}, p_{32}, p_{33}$, etc., of certain types of lesion caused by a certain agent, respectively. Each of these probabilities is similar to N_C introduced above. Then

$$p(1) = \sum_{i,j} p_{ij} \exp(-p_{ij}),$$

$$p(2) = \frac{1}{2} \left[\sum_{i,j} p_{ij}^2 \exp(-p_{ij}) + \sum_{i,j \neq l} p_{ij} \exp(-p_{ij}) p_{il} \exp(-p_{il}) \right], \quad (3)$$

and so forth. These are the probabilities of clustered damage DS1, DS2, etc. The above idea of classification of damage is only attractive if there are not too many terms in the decomposition (3) to be considered. In order to make a judgment about this, we need to analyze the difference between different lesions biologically. For example, let a DSB be inflicted at a certain position in a DNA molecule. SSBs in the same molecule may make up a clustered damage site if they are located close enough to the DSB. Should we distinguish between the situations when SSB is happening 10, 12, or 20 bp away from the DSB? If biologists answer this and similar questions, we can justify (or refute) the

above approach. In order to test the suggested hypothesis, we suggest further study of the repair of particular damage sites. We expect that the number of effective configurations will be limited and the types of clusters will be subdivided into two categories to justify the observed biphasic repair dependence; those (not necessarily the simplest), which are fixed at a fast rate (within two hours) and those (not necessarily the most complex), which are fixed at a slower rate ($\approx 24\text{h}$).

3.3 Effects of thermal and pressure spikes

Now we return to the discussion of pathways of DNA damage. In our works [11,12], we made estimates for the temperature increase in the vicinity of ion tracks. The temperature increase is caused by secondary electrons that get most of the energy lost by the stopping ions. Then, this energy is transferred to the medium as electrons become thermalized and bound. The temperature increase strongly depends on the volume within which the energy is deposited. This volume has been estimated using data on the penetration depth of secondary electrons whose average energy is about 45 eV. The maximum average temperature increase was estimated to be about 100°C , which is enough to denature DNA, but these estimates have been done for a uniform system in thermal equilibrium and the energy transport by electrons before a transfer to the lattice has not been taken into account.

In Ref. [16], we considered the heat transfer during the earliest stage after the ion's passage. The characteristic times of this stage are from 10^{-15} – 10^{-9} s. These times are

longer than the characteristic time of primary ionization (10^{-17} s) and shorter than typical times of conformational changes in DNA such as unwinding, which are measured in μs or even longer times. Nonetheless, the events that happen on this intermediate time scale make the initial conditions for the next scales and may be important for the future dynamics of the medium.

We made calculations using the inelastic Thermal Spike model (i-TS), which was developed to explain track formation in solids irradiated with heavy ions [33,34]. This model studies the energy deposition to the medium by swift heavy ions via secondary electrons. In this model, the strength of the energy transfer from electrons to lattice atoms, called the electron-phonon coupling, is an intrinsic property of the irradiated material. We applied the i-TS model to irradiated liquid water. Fig. 1 [16] presents the temperature of water versus time for a scenario with superheating and $\lambda = 2$ nm for a C-ion beam of 6 MeV or 0.5 MeV/u (LET = 0.91 keV/nm), which corresponds to the energy of carbon ions in the vicinity of the Bragg peak. These results indicate a sharp increase of temperature for a short time. This increase is *much* larger than has been previously estimated in stationary conditions. During the times between 10^{-15} and 10^{-10} s after the ion's passage, the temperature rises considerably at different distances from the ion track [16].

The described system reaches thermalization only by the time of about 10^{-12} s; therefore the temperature, which we discuss above, is rather a distribution of energy per molecule calculated in K. Nevertheless, the energy transfer

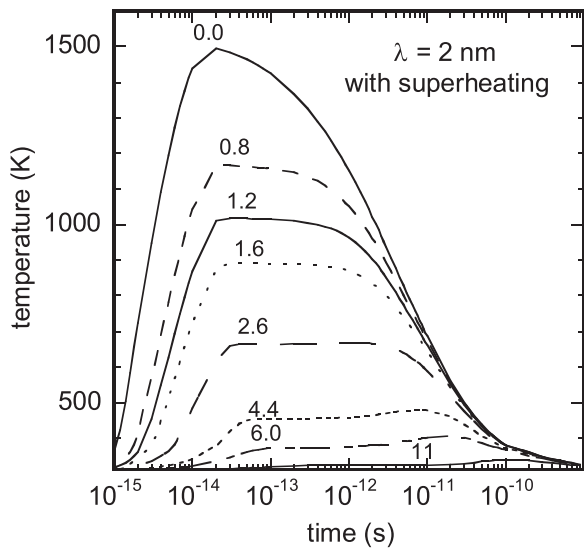


Fig. 1. The temperature on the molecular subsystem versus time for one value of the electron-phonon mean free path ($\lambda = 2$ nm), assuming a superheating scenario. The calculations have been performed for 0.5-MeV/u C ions (LET = 0.91 keV/nm [35]). The calculations are performed for different radii relative to the ion axis. These radii are given (in nm) near each curve.

inevitably takes place near ion tracks and the i-TS model presents a plausible picture of this transient process. A rapid energy transfer between internal degrees of freedom occurs on the femtosecond scale. Then, the energy is transferred to the translational degrees of freedom. If the i-TS model does not correctly reproduce the dynamics of this transition, the temperature spikes may be smaller.

Still, if real, very large temperature and pressure increases (within 10 nm of the ion trajectories, predicted in Ref. [16]) may result in considerable forces acting on DNA. These may be large enough to cause mechanical damage, such as strand breaks, and thus be a separate mechanism of DNA damage during irradiation by ions.

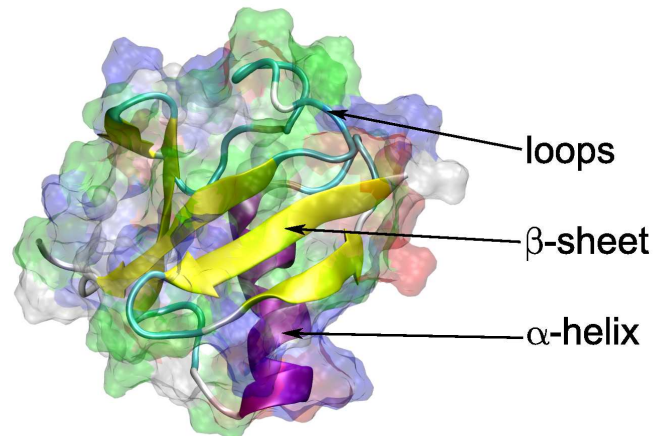


Fig. 2. The structure of protein ubiquitin (PDB ID 1UBQ). The Figure was rendered using VMD program [37]. The elements of the secondary structure are shown by arrows.

3.4 Influence of the thermal spike on proteins structure

In order to investigate the stability of protein structures under ultrafast heating events caused by the propagating heavy ions, we have performed molecular dynamics simulations of proteins exposed to heating events. As a case study, we have chosen the small and well known globular protein ubiquitin. The crystallographic structure of this protein is shown in Fig. 2 and was obtained from the Protein Data Bank [36] using ID code 1UBQ. Ubiquitin consists of 76 amino acids and its main function is associated with the labeling of the proteins in the cell for proteasomal degradation. The choice of ubiquitin as a test example is motivated by the fact that this protein has helix and sheet elements of the secondary structure, being one of the smallest and compact proteins.

The molecular dynamics simulations were performed using the following procedure. The protein with the crystallographic structure was solvated in a water box with the edge size of 80 Å. Water was simulated using the TIP3 parameterization for water molecules. The solvent was ionized with ions of sodium and chloride with concentrations of 100 mM. The molecular dynamics simulations were performed in the NVT ensemble using the NAMD software package [38] and the CHARMM27 forcefield [39], and using a timestep of 1 fs. The temperature control was maintained using a Langevin thermostat with a damping coefficient of 5 ps⁻¹. In order to simulate the heating of the medium by the energetic particle, the temperature of the thermostat was adjusted after each 10 timesteps to the temperature profile shown in Fig. 1. It is important to mention that in the presented calculations, we have not accounted for the spatial dependence of the temperature peak and assumed that the whole system experiences the temperature spike as if it is located on the trajectory of the propagating particle.

We have performed four independent molecular dynamics simulations of ubiquitin exposed to the same heating event. The simulations were performed for the first 300 ps after the ion's passage. As it is seen from Fig. 1, the temperature of the medium at 300 ps after propagation of the energetic particle is lower than 350 K. Therefore, one can speculate that the prominent changes in the secondary structure of the protein caused by the temperature increase should occur during the first 300 ps after

the ion's passage, since, later on the temperature is rather low.

Since we are interested in the influence of the thermal spike on the secondary structure of the protein, in Fig. 3 we present four dependencies of the secondary structure of ubiquitin on time obtained from four independent calculations. On the vertical axis of each plot in Fig. 3 is the index of each amino acid in the protein while the horizontal axis is the time after the propagation of the particle. Each color represents different types of secondary structure: purple represents α -helices, yellow represents β -sheets, green represents loop regions and blue represents π -helices. The white color represents the cases where it is not possible to assign any kind of secondary structure to the amino acids. Thereby, from Fig. 3 one can see which type of secondary structure each amino acid has at a certain period of time.

From Fig. 3, it is seen that the most prominent disturbances of the secondary structure of the protein occur during the first 100 ps after the propagation of the energetic particle. However, during the time between 100 and 300 ps the fluctuations of the secondary structure of the protein decrease. Moreover, it is possible to state that at the end of the simulation ubiquitin drifts back to its native conformation since most of the elements of the secondary structure of the protein are in the conformation corresponding to the native one.

Therefore, from the performed calculations it is difficult to undoubtedly make conclusions about the influence of the thermal spike on the secondary structure of

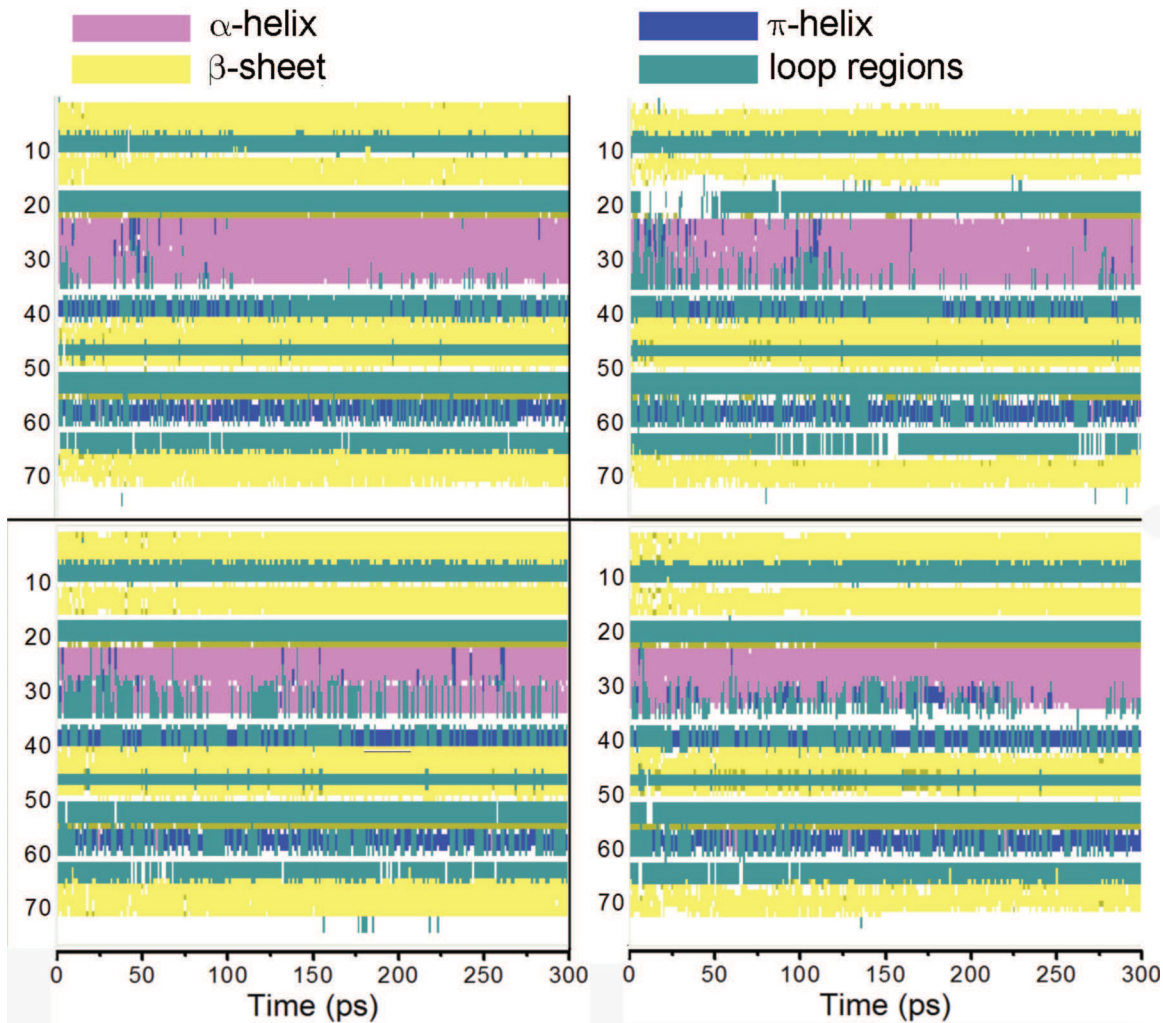


Fig. 3. The dependence of secondary structure of ubiquitin on time in a course of the heating event. The ordinate represents the index of amino acid in the protein. Each color corresponds to different types of secondary structure: purple represents α -helices, yellow represents β -sheets, green represents loop regions and blue represents π -helices. The white color represents the cases where it is not possible to assign any kind of secondary structure to the amino acids. The zero time corresponds to the moment of propagation of the energetic particle.

the protein. However, it is seen that the secondary structure of the protein can be substantially distorted by the thermal spike. But the proteins with fast folding kinetics such as ubiquitin are able to rapidly refold to the native state. Therefore, one can speculate that the most prominent effect of the damage on the secondary structure of the protein should be observed in proteins with a more com-

plicated folding landscape. These kinds of proteins, which are not able to refold themselves on their own, can be considered as the most prone to damage. In the present work, we do not perform the molecular dynamics simulations of proteins obeying slow and complicated folding kinetics due to the large size of these systems and we leave this question open for further considerations.

3.5 Other effects of local heating

Another issue which will have to be addressed is related to chemical changes in the DNA environment and their effects on DNA. It is expected that due to temperature spikes, the rates of chemical reactions increase by orders of magnitude. This concerns the dissociation of water as well as larger molecules. These processes produce more hydroxyl radicals and change the reactivity of the DNA environment. At the same time, DNA itself, which may be partially denaturated, becomes more vulnerable to chemical damage. Temperature spikes affect the probabilities of direct and quasi-direct pathways of DNA damage by means of secondary electrons and holes since the thresholds for some effects (such as vibronic excitation) [40,41,22] are comparable to the energies transferred to the DNA via the heat conductance mechanisms described in Ref. [16]. This means that ionization of DNA with its concurrent heating may be the dominant pathway leading to strand breaks.

4 Conclusions and outlook

In concluding this paper, we want to summarize our achievements in the development of the multiscale approach to radiation damage and outline some perspectives for future developments. First, on the stage of propagation of ions we reproduced the position and shape of the Bragg peak for protons and for carbon ions propagating in water. Several important effects define this stage [12,17]: ionization and excitation of the medium, charge transfer, scattering,

and nuclear fragmentation. The latter has not yet been included in the multiscale approach and we hope to do it in the future. The energy spectra of secondary electrons produced during ionization of the medium have been addressed in refs [12,17] and probably can be further improved. They serve as a starting point for the following stage of the transport of secondaries considered in ref. [14] and heat transfer considered in ref. [16]. The transport stage can be further improved. The result should include the radial distribution of the clustered damage, described in this work. It is essential that the analysis of clusterization be related to investigations of DNA repair, which will one day also become a part of the multiscale approach. The heat transfer stage requires more efforts: the validity of application of the thermal spike model has to be verified. The direct effect on biomolecules should be further investigated using more realistic dynamical conditions. Finally, the other, indirect consequences of thermal spikes have to be explored. Thus, we have probably reached the “end of the beginning”; there is plenty of work yet to be done. We are hopeful that a beautiful physical picture will finally describe the complicated puzzle involved in the phenomena of ion-beam therapy.

Acknowledgments

This work has contributed from discussions with Igor Mishustin, Walter Greiner and those at RADAM 2009. E.S. is grateful to Lynn Harrison and J. S. Payson. The Deutsche Forschungsgemeinschaft support is very much appreciated.

References

1. U. Amaldi, G. Kraft, Rep. Prog. Phys. **68**, 1861 (2005)
2. U. Amaldi, G. Kraft, J. Radiat. Res. **48**, A27 (2007)
3. H. Tsujii, T. Kamada, M. Baba, H. Tsuji, H. Kato, S. Kato, S. Yamada, S. Yasuda, T. Yanagi, H. Kato et al., New J. Phys. **10**, 075009 (2008)
4. J. Kiefer, *Biological Radiation Effects* (Springer-Verlag, Berlin, Heidelberg, New York, 1990)
5. R. Kanaar, J. Hoeijmakers, D. van Gent, Trends Cell Biol. **8**, 483 (1998)
6. D. Frankenberg, M. Frankenberg-Schwager, D. Blöcher, R. Harbich, Radiat. Res. **88**, 524 (1981)
7. D. Goodhead, J. Thacker, R. Cox, Int. J. Radiat. Biol. **63**, 543 (1993)
8. T. Elsaesser, M. Kraemer, M. Scholz, Int. J. Radiat. Oncol. Biol. Phys. **71**, 866 (2008)
9. M. Scholz, A. Kellerer, W. Kraft-Weyrather, G. Kraft, Radiat. Environ. Biophys. **36**, 59 (1997)
10. T. Elsaesser, M. Scholz, Radiat. Res. **167**, 319 (2007)
11. O. Obolensky, E. Surdutovich, I. Pshenichnov, I. Mishustin, A. Solov'yov, W. Greiner, Nucl. Inst. Meth. B **266**, 1623 (2008)
12. E. Surdutovich, O. Obolensky, E. Scifoni, I. Pshenichnov, I. Mishustin, A. Solov'yov, W. Greiner, Eur. Phys. J. D **51**, 63 (2009)
13. E. Scifoni, E. Surdutovich, I. Pshenichnov, I. Mishustin, A. Solov'yov, W. Greiner, *Ion-beam therapy: from electron production in tissue like media to DNA damage estimations*, in *Proceedings of the 5th International Conference (RADAM 2008)*, edited by K. Tokesi, B. Sulik (New York, 2008), Vol. 1080, pp. 104–110
14. A. Solov'yov, E. Surdutovich, E. Scifoni, I. Mishustin, W. Greiner, Phys. Rev. **E79**, 011909 (2009)
15. E. Surdutovich, A. Solov'yov, Europhys. News **40/2**, 21 (2009)
16. M. Toulemonde, E. Surdutovich, A. Solov'yov, Phys. Rev. E **80**, 031913 (2009)
17. E. Scifoni, E. Surdutovich, A. Solov'yov, Phys. Rev. E **81**, in production (2010)
18. D. Becker, M. Sevilla, *The Chemical Consequences of Radiation Damage to DNA*, in *Advances in Radiation Biology*, edited by J. Lett (Acad. Press, 1993), Vol. 17, pp. 121–180
19. D. Becker, A. Adhikary, M. Sevilla, *Physicochemical mechanisms of radiation induced DNA damage (Chapter 20)*, in *Charged Particle and Photon Interactions with Matter Recent Advances, Applications, and Interfaces* (CRC Press, Taylor & Francis, Boca Raton, 2010)
20. A. Kumar, M. Sevilla, *Theoretical modeling of radiation-induced DNA damage*, in *Radical and radical ion reactivity in nucleic acid chemistry*, edited by M. Greenberg (J. Wiley & Sons, Inc., New York, 2009), p. 1
21. L. Sanche, Eur. Phys. J. D **35**, 367 (2005)
22. A. Adhikary, A. Kumar, M. Sevilla, Radiat. Res. **165**, 479 (2006)
23. J. Ward, Prog. Nucleic Acid. Res. Mol. Biol. **35**, 95 (1988)
24. J. Ward, Radiat. Res. **142**, 362 (1995)
25. M. Dingfelder, D. Hantke, M. Inokuti, H. Paretzke, Radiat. Phys. Chem. **53**, 1 (1998)
26. H. Nikjoo, S. Uehara, D. Emfietzoglou, F.A. Cucinotta, Radiat. Meas. **41**, 1052 (2006)
27. C. Tung, T. Chao, H. Hsieh, W. Chan, Nucl. Inst. Meth. B **262**, 231 (2007)

28. B. Jakob, M. Scholz, G. Taucher-Scholz, *Radiat. Res.* **159**, 676 (2003)
29. S. Malyarchuk, R. Castore, L. Harrison, *DNA Repair* **8**, 1343 (2009)
30. S. Malyarchuk, R. Castore, L. Harrison, *Nucleic Acids Res.* **36**, 4872 (2008)
31. Y. Hsiao, R. Stewart, *Phys. Med. Biol.* **53**, 233 (2008)
32. V. Semenenko, R. Stewart, *Phys. Med. Biol.* **51**, 1693 (2006)
33. M. Toulemonde, W. Assmann, C. Dufour, A. Meftah, F. Studer, C. Trautmann, *Mat. Fys. Medd.* **52**, 263 (2006)
34. A. Meftah, J.M. Costantini, N. Khalfaoui, S. Boudjadar, J.P. Stoquert, F. Studer, M. Toulemonde, *Nucl. Instr. Meth. B* **237**, 563 (2005)
35. J.F. Ziegler, *Nucl. Instr. Meth. B* **219-200**, 1027 (2003)
36. <http://www.rcsb.org/> (2009)
37. W. Humphrey, A. Dalke, K. Schulten, *J. Molec. Graphics* **14**, 33 (1996)
38. J.C. Phillips, R. Braun, W. Wang, *et al*, *J. Comp. Chem.* **26**, 1781 (2005)
39. A. MacKerell, D. Bashford, R. Bellott, *et al*, *J. Phys. Chem. B* **102**, 3586 (1998)
40. A. Kumar, M. Sevilla, *J. Phys. Chem. B* **111**, 5464 (2007)
41. A. Kumar, M. Sevilla, *J. Am. Chem. Soc.* **130**, 2131 (2008)